JACS
JOURNAL OF THE AMERICAN CHEMICAL SOCIETY
Article

Heterogeneous Catalysts Need Not Be so "Heterogeneous": Monodisperse Pt Nanocrystals by Combining Shape-Controlled Synthesis and Purification by Colloidal Recrystallization

Yijin Kang,[†] Meng Li,[§] Yun Cai,[§] Matteo Cargnello,[†] Rosa E. Diaz,[∥] Thomas R. Gordon,[†] Noah L. Wieder,[⊥] Radoslav R. Adzic,[§] Raymond J. Gorte,[⊥] Eric A. Stach,[∥] and Christopher B. Murray*[,†,‡]

[†]Department of Chemistry, University of Pennsylvania, Philadelphia, Pennsylvania 19104, United States
[‡]Department of Materials Science and Engineering, University of Pennsylvania, Philadelphia, Pennsylvania 19104, United States
[§]Department of Chemistry, Brookhaven National Laboratory, Upton, New York 11973, United States
[∥]Center for Functional Nanomaterials, Brookhaven National Laboratory, Upton, New York 11973, United States
[⊥]Department of Chemical and Biomolecular Engineering, University of Pennsylvania, Philadelphia, Pennsylvania 19104, United States

Supporting Information

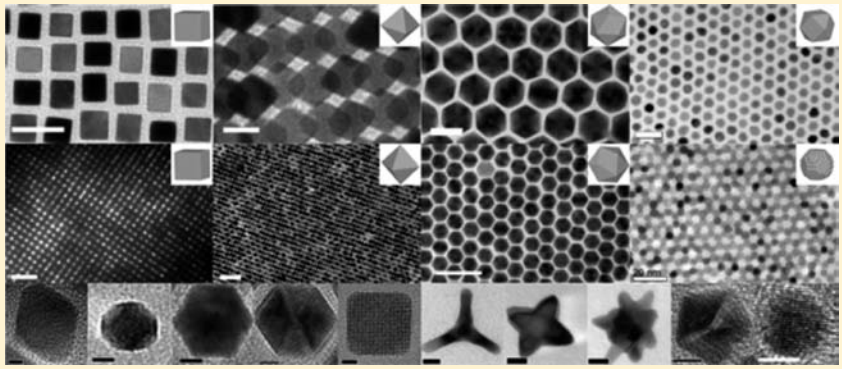

ABSTRACT: Well-defined surfaces of Pt have been extensively studied for various catalytic processes. However, industrial catalysts are mostly composed of fine particles (e.g., nanocrystals), due to the desire for a high surface to volume ratio. Therefore, it is very important to explore and understand the catalytic processes both at nanoscale and on extended surfaces. In this report, a general synthetic method is described to prepare Pt nanocrystals with various morphologies. The synthesized Pt nanocrystals are further purified by exploiting the "self-cleaning" effect which results from the "colloidal recrystallization" of Pt supercrystals. The resulting high-purity nanocrystals enable the direct comparison of the reactivity of the {111} and {100} facets for important catalytic reactions. With these high-purity Pt nanocrystals, we have made several observations: Pt octahedra show higher poisoning tolerance in the electrooxidation of formic acid than Pt cubes; the oxidation of CO on Pt nanocrystals is structure insensitive when the partial pressure ratio p_{O2}/p_{CO} is close to or less than 0.5, while it is structure sensitive in the O_2-rich environment; Pt octahedra have a lower activation energy than Pt cubes when catalyzing the electron transfer reaction between hexacyanoferrate (III) and thiosulfate ions. Through electrocatalysis, gas-phase-catalysis of CO oxidation, and a liquid-phase-catalysis of electron transfer reaction, we demonstrate that high quality Pt nanocrystals which have {111} and {100} facets selectively expose are ideal model materials to study catalysis at nanoscale.

INTRODUCTION

In recent decades, the explosive growth of nanoscience has allowed researchers to implement the knowledge learned from surface science studies on well-defined single crystals into nanosized real catalysts.[1] Engineering the shape of nanocrystals is one important aspect of this strategy.[2−18] Pt nanocrystals have received particularly intensive attention because Pt is utilized in many catalytic processes. Numerous attempts of the shape-controlled synthesis of Pt nanocrystals have been reported[2−5,7,8,19−24] since the pioneering work of El-Sayed et al. in 1996;[2,25] and a number of structure sensitive reactions have been described. For example, Feliu et al. reported shape-dependent methanol and formic acid electrooxidation on preferentially oriented Pt nanoparticles,[9] Zaera et al. described tuning the selectivity of isomerization reactions by controlling the particle shape of Pt,[11] and Somorjai et al. demonstrated the shape effects of Pt nanocrystals on benzene hydrogenation selectivity.[5] Well-controlled synthesis of nanocrystals is critical to correlate structural properties (size, shape, and composition)

Received: November 29, 2012
Published: January 27, 2013

   dx.doi.org/10.1021/ja3116839 | J. Am. Chem. Soc. 2013, 135, 2741−2747

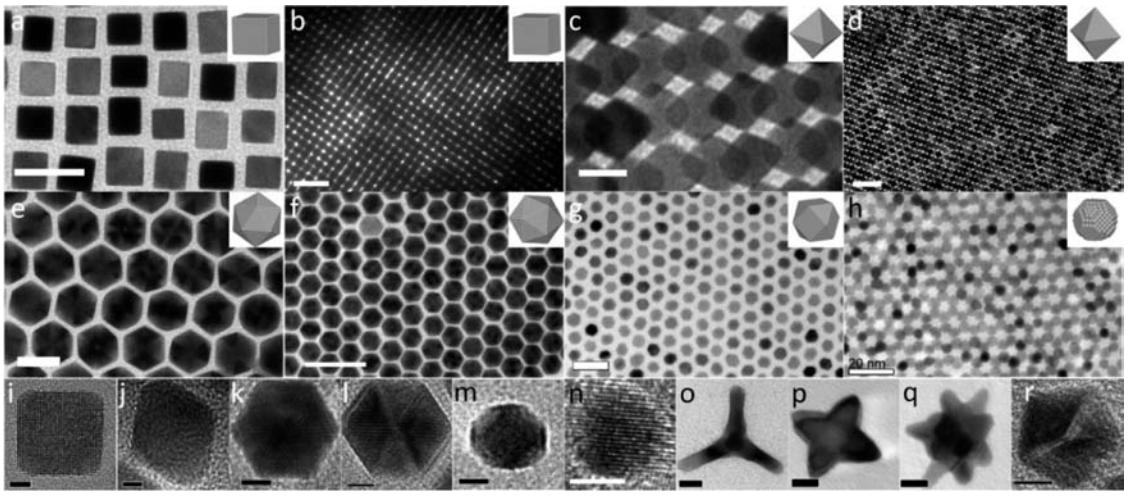

Figure 1. TEM images of (a, b) Pt cubes, (c, d) Pt octahedra, (e, f) Pt icosahedra, (g) Pt cuboctahedra, (h) Pt spheres, and HRTEM images of Pt nanocrystals in the morphologies of (i) cube, (j) octahedron, (k, l) icosahedron, (m) truncated cube, (n) sphere, (o) tetrapod, (p) star-like octapod, (q) multipod, (r) 5-fold twinned decahedron. Scale bars: (a, e, g, h) 20 nm, (b, d, f) 50 nm, (c, o, p, q) 10 nm, 100 nm, (i, j) 2 nm, (k, l, m, n, r) 5 nm.

with catalytic performance.[1,26−39] Recently, near perfect shape control at the size scale of 100−300 nm has been achieved in Au,[12] Ag,[12,16] Pt,[12] and Pd[12] nanocrystals, but the preparation of well-controlled Pt nanocrystal at the sub-20 nm size scale which is of particular interest in catalysis, is still highly challenging.

The (111) and (100) surfaces are the most common low-index surfaces of Pt nanocrystal and an isotropically grown Pt particle is mostly covered by {111} and {100} facets. Therefore, to design a new generation of catalysts with high performance, it is crucial to understand the catalytic properties of {111} and {100} in real catalysts for various structure sensitive reactions. While nearly monodisperse Pt nanocubes exposing {100} facets can be synthesized by several methods;[4,5,14,19−21,25] highly controlled synthesis of monodisperse Pt nanocrystals exposing {111} facets has not been reported to date, although ensembles of particles expressing predominantly {111} facets have been made by several pioneering groups.[2−4,9] Until now, scientists have used statistical analysis to attribute the properties to a distribution of shapes and sizes within the samples,[3,9,11] or indirectly compared the structure-sensitive reactions on the cubes, with {100} facets, to an alternate shape with both {111} and {100} facets (e.g., cuboctahedra and spheres).[5,13] Their success has enabled the identification of many important structure sensitive reactions; however, the direct comparison of {111} and {100} has not been possible to date.

Combined with shape-controlled synthesis, purification by colloidal recrystallization provides a powerful strategy for the isolation of high quality nanocrystals with narrow size and shape distributions. Ever since size-selective-precipitation was employed to purify quantum dots (i.e., nanocrystals),[40,41] researchers have paid particular attention to the size,[42−44] shape,[44−46] and even crystallinity segregation[47] in nanocrystals. In this report, we produce nearly monodisperse Pt nanocrystals in various morphologies via solution-phase-synthesis and a unique purification technique which exploits the nanocrystals natural tendency to self-organize to allow purification by colloidal recrystallization. The resulting high-purity nanocrystals enable the direct comparison of the reactivity on {111} and {100} facets for important catalytic reactions.

EXPERIMENTAL SECTION

Synthesis and Characterization of Nanocrystals. Details are described in the Supporting Information.

Purification of Nanocrystals by Colloidal Recrystallization. Equal volume of ethanol is slowly added into a hexane solution of colloidal nanocrystals to form a two-phase solution (upper layer: hexane solution of nanocrystals, lower layer: colorless ethanol). The container is sealed and the supercrystals are allowed to nucleate and grow at the interface of two solution layers for approximately 1−2 week. Then the solvent is allowed to slowly evaporate over approximately 1−2 weeks. At this stage, the nanocrystal solution is crystallized on the existing supercrystals. After that, the solids are transferred onto a piece of filter paper, and washed with a few drops of hexane. Hexane dissolves the out layer, and is absorbed by the filter paper. The remaining solids are collected and redissolved in hexane to form a highly pure nanocrystal solution. Notably, the nanocrystals absorbed in filter paper can also be redissolved in hexane. In this way, the materials (here, nanocrystals) are 100% recyclable.

Electrochemical Measurements. Details are described in the Supporting Information.

CO Oxidation. Pt nanocrystals are loaded on Al_2O_3 at an approximate loading of 1%. The actual loading is determined by ICP-OES. CO oxidation measurements are carried out in a flow-reactor at a GHSV of 15,000 $mLh^{-1}g^{-1}Pt$, and are detected with a gas chromatography (GC) equipped with a thermal conductivity detector (TCD). The conversion is controlled below 20%. p_{O2}/p_{CO} = 1 (1% CO, 1% O_2); p_{O2}/p_{CO} = 40 (1% CO, 40% O_2); p_{O2}/p_{CO} = 0.025 (40% CO, 1% O_2), rest He.

Electron-Transfer Reaction. The experiments are performed according to literature,[3,48,49] except Al_2O_3 supported Pt nanocrystals are used as catalysts. Details are described in the Supporting Information, SI.

RESULTS AND DISCUSSION

Shape-Controlled Synthesis of Pt Nanocrystals. The Pt nanocrystals are synthesized using Pt acetylacetonate as the source of Pt, oleic acid, and oleylamine (oleylamine is also cosolvent) as capping agents, and CO gas and/or metal carbonyls as additives. Various solvents are used to dissolve the metal carbonyls prior to injection. Interestingly, we observe that when chloroform is used, pure Pt nanocrystals are produced, whereas using benzyl ether or any other solvents (such as hexane, dichlorobenzene, toluene, and etc.) results in Pt-metal

dx.doi.org/10.1021/ja3116839 | J. Am. Chem. Soc. 2013, 135, 2741−2747

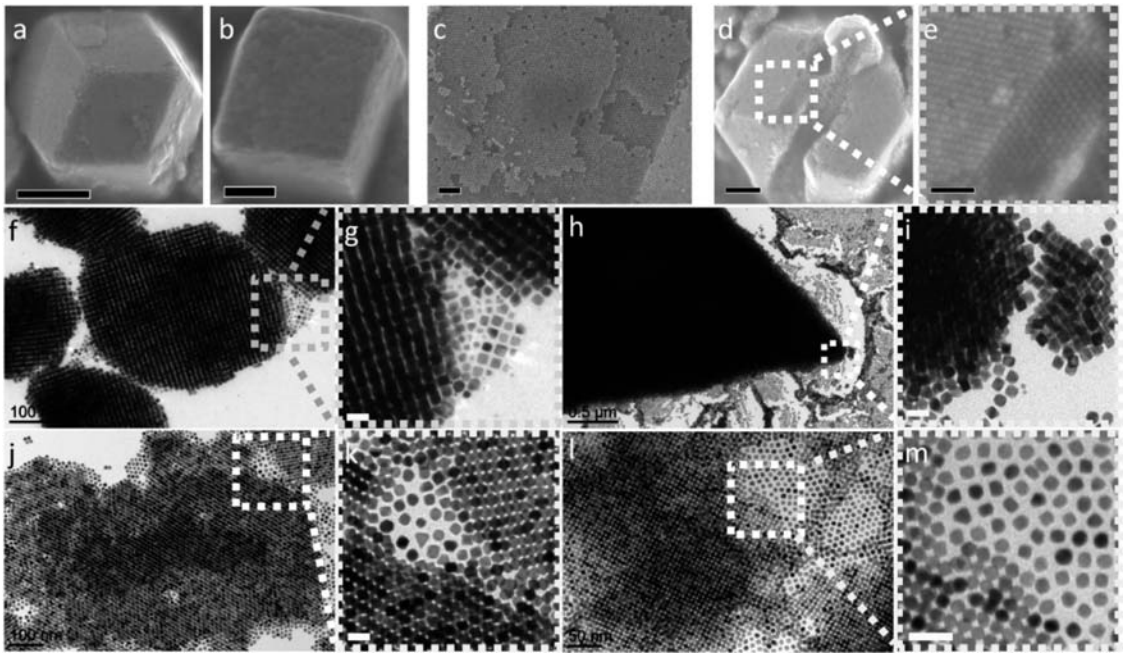

Figure 2. SEM images of (a) rhombic dodecahedral supercrystal self-assembled from octahedral Pt nanocrystals, (b) cubic supercrystal self-assembled from cubic Pt nanocrystals, (c) surface of rhombic dodecahedral supercrystal covered by highly monodisperse Pt octahedra, (d) a supercrystal with a scratch. TEM images of self-assembled (f) cubes, (h, j) octahedra, (l) truncated cubes. Images of e, g, i, k, and m are magnified views of the regions indicated in d, f, h, j, and l respectively. Scale bars: (a, h) 500 nm, (b, d) 200 nm, (c, e, f, j) 100 nm, (g, i, k, m) 20 nm, (l) 50 nm.

alloys.[13] In this study, we use a chloroform solution of dimanganese decacarbonyl as an additive to control the shape of Pt nanocrystals and to prevent alloying. The shape of Pt nanocrystals is highly sensitive to the reaction temperature: at 180−190 °C, a mixture of icosahedra and cubes is formed; at 190−210 °C, a mixture of icosahedra and truncated cubes is produced; at 210−230 °C, octahedra are main product; and above 230 °C, only cubes are produced. During the synthesis of Pt octahedra, trace amounts of icosahedra, triangular plates, and 5-fold twin defects are also observed. Increasing the ratio of Pt:carbonyls leads to cuboctahedra, and the synthesis at the ratio of Pt:Mn = 1:2 produces small Pt nanocrystals which are nearly spherical. In contrast, benzyl ether solutions of dimanganese decacarbonyl generate more pronounced mixtures (stars, branched structures), along with Mn−Pt nanocubes. Due to the limited scope of this report, the detailed synthesis and possible mechanisms are described elsewhere.[50]

Figure 1 presents images of shape-controlled Pt nanocrystals. Pt nanocubes exposing {100} facets can be synthesized either using gaseous CO (Figure 1a) or Mn carbonyl (Figure S1 of the SI). The nanocubes, as shown in Figure 1a, have an average edge length of 9.3 nm (σ = 6%) and they have flat {100} facets and sharp corners. Due to the relatively large initial size-distribution (σ = 10%), the nanocubes synthesized using CO can only be assembled into large-area superlattices (Figure 1b) after a size-selective purification (σ = 6%). Figure 1c shows the image of Pt octahedra which display {111} facets and have a 12.6 nm vertex to vertex distance (σ < 5%). The Pt octahedra readily form superlattices with a crystalline packing referred to as the Minkowski lattice, as shown in Figure 1d. Figure 1e,f depicts the nearly monodisperse Pt icosahedra, which have a size of 20.4 nm (vertex to vertex distance, σ < 5%) and also have their {111} facets exposed. Figure 1g exhibits the 7.0 nm (σ = 5%) Pt cuboctahedra and Figure 1h shows the near spherical Pt nanocrystals with a diameter of 4.7 nm (σ < 5%). Figure 1i−r shows the high-resolution transmission electron microscope (HRTEM) images of cube, octahedron, icosahedra, truncated-cube, sphere, tetrapod, star-like octapod, multipod, and an observed 5-fold twinned Pt nanocrystals.

"Self-Cleaning" Effect in the Colloidal Recrystallization of Nanocrystals. After solution-phase synthesis, especially when mixtures of morphologies are generated, a purification process is necessary to obtain highly uniform nanocrystals. The most popular method of purification is the so-called size-selective-precipitation (SSP) process.[41,51] Adding a nonsolvent into colloid mixtures fractionates the colloid based on size and shape. SSP is particularly effective when different components in the mixture are distinctively different in size and shape. For example, it is quite easy to separate the larger icosahedra from the smaller cubes or truncated cubes, or to purify a spherical Pt nanocrystal by removing extra small particles. However, SSP is not as effective if the components are very similar to each other, both in size and shape (e.g., separating 8 nm truncated cubes from 9 nm cubes). Moreover, it is difficult to further improve a size/shape distribution by SSP if the distribution is already narrow (i.e., σ = 5%). Beyond this point, a more effective separation method is highly desirable.

Uniform nanocrystals are known to self-assemble into crystalline superlattice domains, also referred to as supercrystals, colloidal crystals, or mesocrystals, upon deposition under appropriate conditions.[52,53] We observe that the nanocrystals self-assembled into superlattices are highly uniform in both size and shape, while the irregular shaped nanocrystals are excluded from the self-assembled superlattices. Examples of this phenomenon are presented in Figure 2. Pt octahedra and Pt cubes can self-assemble into supercrystals that grow in the shapes of rhombic dodecahedron (Figures 2a and S2 of the SI) and cube (Figure 2b), respectively. The nanocrystals which form the supercrystal are highly uniform (σ < 3%), both on the surface (Figures 2c and S3 of the SI) and

dx.doi.org/10.1021/ja3116839 | J. Am. Chem. Soc. 2013, 135, 2741−2747

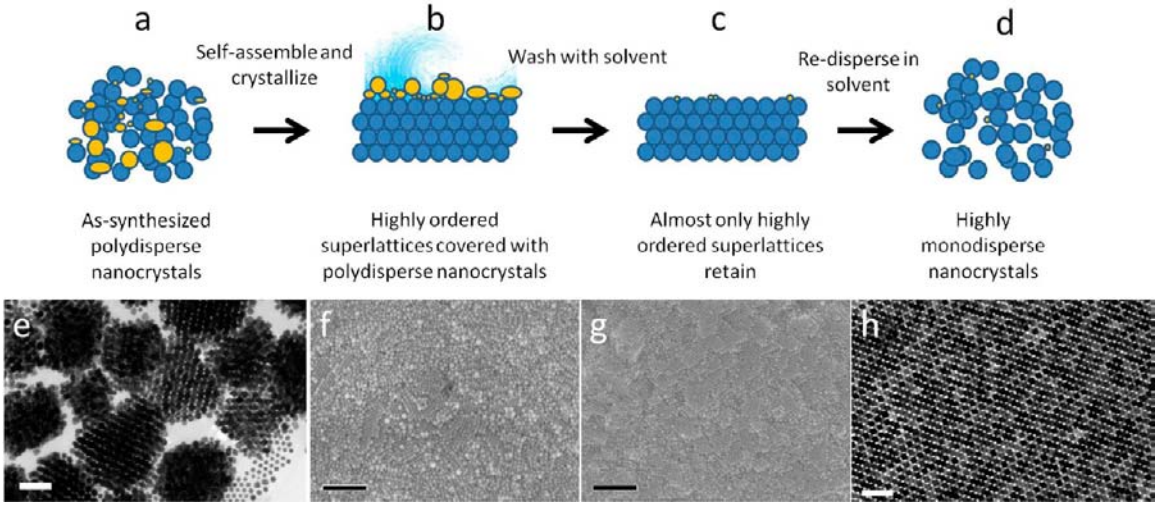

Figure 3. (a–d) Illustration of the purification procedure utilizing the "self-cleaning" effect of nanocrystals. (e, h) TEM and (f, g) SEM images of e–h corresponding to the steps of a–d, respectively. Scale bars: (e, h) 50 nm, (f, g) 200 nm.

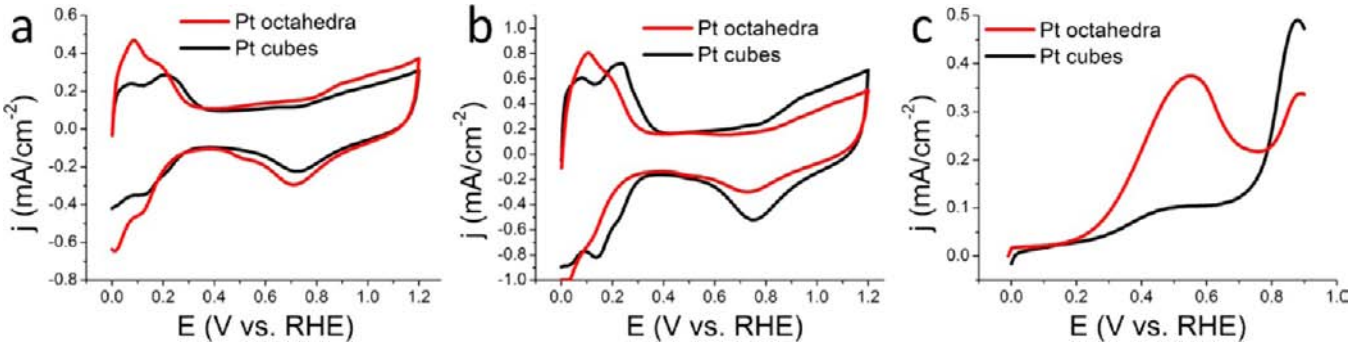

Figure 4. CV curves of Pt octahedra and Pt cubes in (a) $HClO_4$ and (b) H_2SO_4, and (c) polarization curves of electrocatalysis for formic acid oxidation.

within the interior (Figure 2d,e) of supercrystals. Figure 2f,g shows that irregular cubes and small nanocrystals are excluded from the ordered cubic arrays at the edge of superlattice of Pt nanocubes. Figure 2h,j shows the assembled Pt octahedra. The majority of Pt octahedra assemble into large supercrystals (Figure 2h) or superlattice films which are a few layers thick (Figure 2j), while the byproducts (impurities) such as cubes, truncated cubes, truncated octahedra, icosahedra, and triangular plates are excluded from the formation of ordered self-assemblies (Figure 2i,k). Similarly, in the assembly of truncated-cubes, the phase-segregation is also observed (Figure 2l,m). The phase-segregation (size-segregation and shape-segregation) phenomenon results from the maximization of dispersion attraction and packing density, and minimization of the free energy, as described in previous reports.[16,42,43,54−56]

We develop a method to utilize this phase-segregation induced "self-cleaning" to further purify nanocrystals (Figure 3). As illustrated in Figure 3a, the solution of nanocrystals obtained from the purification of SSP contains a portion of irregular or undesirable nanocrystals (impurities). A solution of nanocrystals is allowed to solidify and crystallize at a very slow rate (crystallized in 2–4 weeks). During the crystallization process, the nanocrystals form ordered supercrystals covered with a layer of irregular nanocrystals which are excluded from the formation of ordered crystalline assemblies (Figure 3b). A brief rinsing of the solid with drops of solvent such as hexane allows most of the irregular nanocrystals on the surface of the supercrystals to be resuspended and washed away (Figure 3c). The remaining solids are then collected and redissolved in solvent to form a solution of highly monodisperse nanocrystals (Figure 3d). For instance, the as-synthesized product of Pt octahedra usually contains 70–80% nanocrystals with the octahedral morphology (Figure 3e). The octahedra can self-assemble into a supercrystal and the nonoctahedral nanocrystals deposit on the surface of supercrystals (Figures 3f and S7 of the SI). After washing with hexane, the surface of remaining solid shows ordered, faceted structures (Figures 3g and S8 of the SI). After the complete purification process, the percentage of octahedra is close to 100%, (σ = 5%, purity = 99% in Figure 3h). Thus, the proportion of (111) surface on the nanocrystals is maximized, making them an excellent model for the (111) surface in the study of catalysis. Here, the Pt nanocrystals with various morphologies have the highest quality reported up to date, and are highly suitable for studying structure sensitive reactions.

Electrocatalysis. Many electrocatalytic processes are dependent on the surface structure of electrocatalysts. As early as 1981, Adzic et al. and Clavilier et al. reported that the electrooxidation of formic acid, methanol, and formaldehyde is structure sensitive to the surface crystallographic orientation of Pt single crystal electrode.[57−59] More recently, Feliu et al. carried out the similar measurements on preferentially oriented Pt nanoparticles.[9] Here, we revisit formic acid oxidation reaction using our well-controlled Pt nanocrystals.

dx.doi.org/10.1021/ja3116839 | J. Am. Chem. Soc. 2013, 135, 2741−2747

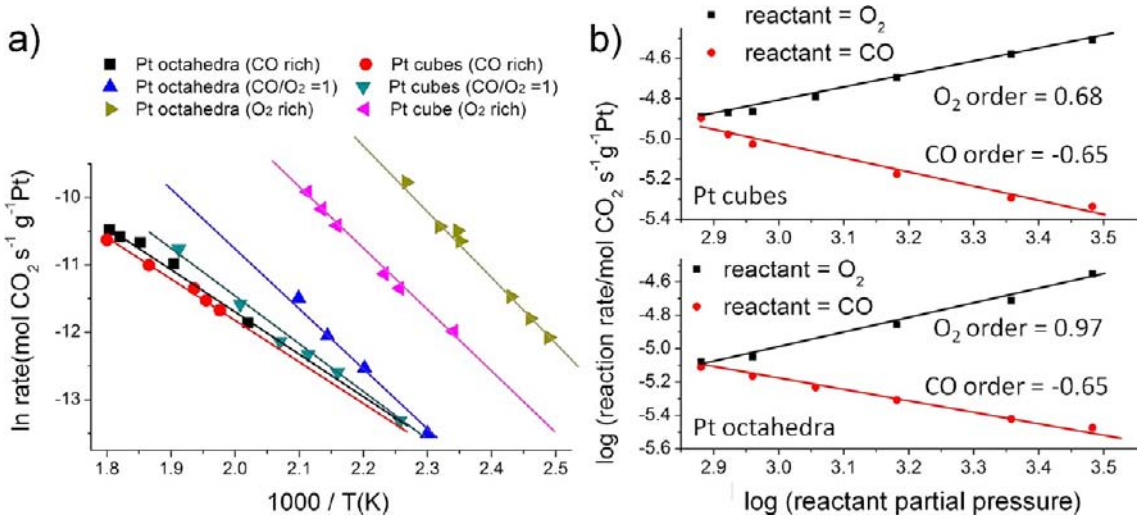

Figure 5. (a) The Arrhenius plots for CO oxidation on Pt nanocrystals. (b) The reactant partial pressure dependence on Pt cubes and Pt octahedra (when one reactant changes in partial pressure, the other one is always kept at 7.6 Torr). The determination of reaction orders are carried out at 195−200 °C.

Figure 4a,b show typical cyclic voltammetry (CV) curves for the Pt cubes and octahedra in 0.1 M $HClO_4$ and 0.1 M H_2SO_4, respectively. In the voltammetric curves recorded in 0.1 M H_2SO_4 (Figure 4b), the hydrogen underpotential deposition (H UPD) profiles of the two nanocrystals show distinct difference, which can be correlated to their different surface structures. The more positive H adsorption/desorption potential as well as the pair of peaks showing at the region of 0.15−0.25 V from the voltammogram of Pt cubes is due to the characteristic H-adsorption features at Pt{100} planes. A pair of small bumps in the region of 0.4−0.6 V (Figure 4b), corresponding to the characteristic "butterfly peaks" in the voltammogram of Pt(111), is observed from Pt octahedra CV. The significantly suppressed intensity of the "butterfly peaks" can be explained by the increased amount of atoms at edges and corners and consequently lowered orderliness on the Pt octahedral nanocrystals compared to the well-defined Pt(111) single crystal. In the surface hydroxyl formation region, the Pt cubes display a negatively shifted onset of oxidation and also an increased intensity as compared with the Pt octahedra, which is consistent with the stronger binding of OH species on Pt(100) than that on Pt(111). All of these electrochemical features on the voltammetric curves of Pt nanocrystals fit with expectations with the structural properties revealed by HRTEM (Figure S10). In $HClO_4$, the above features in the CV curves are slightly less apparent but still observable. Figure 4c shows the polarization curves for formic acid oxidation. As the adsorption of poisoning species is lowest on Pt(111) and highest on Pt(100), the Pt octahedra with (111) surface exhibit higher activity than the Pt cubes with (100) facets in the anodic sweep.[57]

CO Oxidation. CO oxidation of Pt surface has been long regarded as a structure insensitive reaction. According to the most accepted Langmuir−Hinshelwood mechanism, CO oxidation involves the adsorbed species of CO (CO_{ads}) and O (O_{ads}).[60] Assuming that the dominant surface species is CO_{ads}, which is realized when the partial pressure ratio p_{O2}/p_{CO} is close to or less than 0.5, the reaction rate can be approximately expressed as follows:[61]

$$d[CO_2]/dt = k\exp(-E_{CO,des}/RT)p_{O2}/p_{CO}$$

where k is the temperature independent constant, $E_{CO,des}$ is the desorption energy of CO. At high CO coverage (i.e., CO_{ads} is dominant at the surface), $E_{CO,des}$ shows little difference regarding different crystal face. Thus, the reaction of CO oxidation is structure insensitive at p_{O2}/p_{CO} close or less than 0.5, as earlier studies indicated.[60,61]

Using our high quality Pt cubes and Pt octahedra as the model of Pt(100) and Pt(111) at nanoscale, we test the CO oxidation at p_{O2}/p_{CO} = 1, 40 (i.e., ≫1), and 0.025 (i.e., ≪1). The results are presented in Figure 5a. In a CO-rich environment, CO oxidation on Pt nanocrystals is observed to be structure insensitive and reactions on both Pt octahedra and cubes have an apparent activation energy of 50.76 ± 3.62 kJmol^{-1}. At p_{O2}/p_{CO} = 1, the reaction can still be considered as structure insensitive, although a slight difference is observed. In O_2-rich environment, the CO oxidation on Pt nanocrystals is clearly structure sensitive, where Pt octahedra possess higher activity than Pt cubes under identical reaction conditions. The CO oxidation on Pt octahedra and Pt cubes under O_2-rich environment show an apparent activation energy of 80.85 ± 5.02 kJmol^{-1} in both cases. The reaction orders are also determined: On both Pt cubes and Pt octahedra, CO shows a negative order of −0.65. The reaction order in O_2 is 0.97 on Pt octahedra and 0.68 on Pt cubes, implying that the activity of CO oxidation reaction increase faster on Pt octahedra than on Pt cubes with increasing O_2 partial pressure. This is consistent with our observation that CO oxidation is structure sensitive on Pt nanocrystals under O_2-rich environment.

Under CO-rich conditions, CO is the dominant adsorbed species on the surface of Pt, so desorption of CO_{ads} is the rate-limiting step in order to open adsorption sites for O_2.[60,62,63] Such desorption process is independent of the surface structure of Pt, thus, the CO oxidation is structure insensitive on Pt under CO-rich conditions. However, in O_2-rich environments the situation becomes very different: the surface of Pt is covered by a mixed phase with CO_{ads} and O_{ads}, thus, desorption of CO_{ads} is no longer the rate-limiting step.[64] Some researchers believe that under O_2-rich environment, Pt may form certain oxides which act as the highly active phase, although others believe Pt cannot be oxidized under these reaction conditions.[61] Nanocrystals possess much less perfect (111) or (100) terraces,

dx.doi.org/10.1021/ja3116839 | J. Am. Chem. Soc. 2013, 135, 2741−2747

but rather a much higher population of low-coordinated Pt atoms.[65] Many factors can contribute to the structure sensitivity in O_2-rich environments. The CO oxidation on Pt at the nanoscale certainly deserves further investigation. Nonetheless, our results indicate that on Pt nanocrystals, CO oxidation could be structure sensitive under O_2-rich environment and the reaction mechanisms at different reaction conditions could be very different.

During the course of the reactions, the Pt nanocrystals show little change in morphology (Figure S11 of the SI). However, with a reaction temperature higher than 250 °C, the morphologies of Pt nanocrystals could change significantly (Figure S12 of the SI). The extented reaction time (e.g., more than 20 h) also destroys the morphology of Pt nanocrystals, even under a mild reaction temperature as low as 100 °C. We are currently utilizing an in situ TEM to understand more about the change in morphology under reaction conditions.

Electron Transfer Reaction. One of the first experiments conducted by the researchers who synthesized shape-controlled Pt nanocrystals was the classic electron transfer reaction between hexacyanoferrate (III) and thiosulfate ions.[3,48,49] Here, we revisit the same reaction with our high quality Pt nanocrystals. In previous reports, El-Sayed et al. have found that tetrahedral Pt nanoparticles which primarily possess Pt {111} facets have a lower activation energy than cubic Pt nanoparticles which preferentially expose their {100} facets.[3,48,49] We observe the same trend, as shown in Figure 6. In this case, the reaction on Pt octahedra shows an activation energy of 7.40 ± 1.78 kJmol^{-1}, which is lower than that observed on Pt cubes, 32.17 ± 1.29 kJmol^{-1}. This demonstration again reinforces the benefit of utilizing our high quality Pt nanocrystals as model materials to study various catalytic processes.

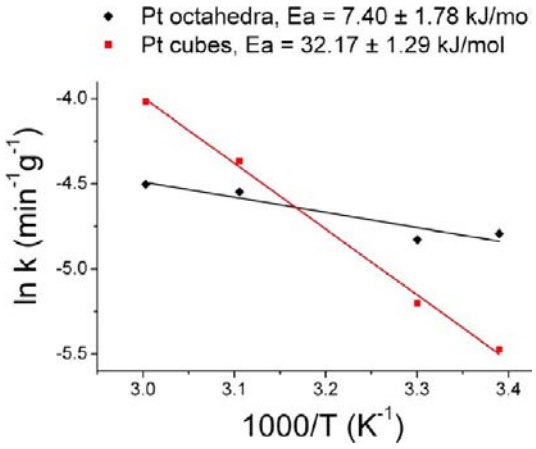

Figure 6. The Arrhenius plots obtained using Pt octahedra and Pt cubes to catalyze the electron transfer reaction between hexacyanoferrate (III) ions and thiosulfate ions.

CONCLUSIONS

In summary, we report a synthetic system using dimanganese decacarbonyl to control the shape of Pt nanocrystals. In this system, monodisperse Pt nanocrystals can be synthesized in various morphologies, including octahedra, icosahedra, cubes, truncated cubes, cuboctahedra, spheres, tetrapods, star-shape octapods, and multipods. We utilize the "self-cleaning" effect of nanocrystals during colloidal recrystallization to further purify the Pt nanocrystals to highest purity in terms of shape available to date. Through electrocatalysis, gas-phase-catalysis of CO oxidation, and liquid-phase-catalysis of electron transfer reaction, we demonstrate high quality Pt nanocrystals which selectively expose {111} or {100} facets are ideal model materials to study catalysis at nanoscale.

ASSOCIATED CONTENT

Supporting Information

Experimental procedures describing synthesis of Pt cubes, octahedra, truncated cubes and icosahedra, cuboctahedra, spheres, tetrapods, and star-like octapods (and multipods); characterizations; electrochemical measurements; electron-transfer reactions; sizes and shape purities of nanocrystals before and after purifications (Table S1); as-synthesized Pt cubes using $Mn_2(CO)_{10}$ (Figure S1); SEM images of supercrystals built with Pt octahedra (Figure S2); SEM images showing the surface of Pt supercrystals built with (a) cubes and (b) octahedra (Figure S3); TEM image of self-assembled Pd NCs (Figure S4); SEM image of poly-oriented supercrystals (Figures S5−S9); TEM images and fast Fourier transform of Pt octahedron and cube (Figures S10); TEM images showing morphological changes (Figure S11,12); Absorption spectra used to monitor the electron-transfer reaction (Figure S13); and TEM image showing the impurities washed off the supercrystals of Pt octahedra (Figure S14). This material is available free of charge via the Internet at http://pubs.acs.org.

AUTHOR INFORMATION

Corresponding Author

cbmurray@sas.upenn.edu

Notes

The authors declare no competing financial interest.

ACKNOWLEDGMENTS

C.B.M. and Y.J.K. acknowledge the partial support from the National Science Foundation MRSEC DMR11-20901. C.B.M. thanks the Richard Perry University Professorship for the support of his supervisor role. N.L.W. and R.J.G. acknowledge support from the Department of Energy, Office of Basic Energy Sciences, Chemical Sciences, Geosciences and Biosciences Division, Grant DE-FG02-85ER13350. Research carried out in part at Department of Chemistry and the Center for Functional Nanomaterials (CFN), Brookhaven National Laboratory (BNL), which is supported by the U.S. Department of Energy, Office of Basic Energy Sciences, under Contract No. DE-AC02-98CH10886. We thank Charles Black and Fernando Camino (CFN, BNL) for the support at CFN, Douglas Yates for the support at the Penn Regional Nanotechnology Facility, and David Vann at Department of Earth and Environmental Science (University of Pennsylvania) for assistance in ICP-OES.

REFERENCES

(1) Li, Y.; Somorjai, G. A. *Nano Lett.* **2010**, *10*, 2289−2295.
(2) Ahmadi, T. S.; Wang, Z. L.; Green, T. C.; Henglein, A.; El-Sayed, M. A. *Science* **1996**, *272*, 1924−1926.
(3) Narayanan, R.; El-Sayed, M. A. *Nano Lett.* **2004**, *4*, 1343−1348.
(4) Song, H.; Kim, F.; Connor, S.; Somorjai, G. A.; Yang, P. D. *J. Phys. Chem. B* **2005**, *109*, 188−193.
(5) Bratlie, K. M.; Lee, H.; Komvopoulos, K.; Yang, P. D.; Somorjai, G. A. *Nano Lett.* **2007**, *7*, 3097−3101.

(6) Habas, S. E.; Lee, H.; Radmilovic, V.; Somorjai, G. A.; Yang, P. D. *Nat. Mater.* **2007**, *6*, 692−697.
(7) Ren, J.; Tilley, R. D. *Small* **2007**, *3*, 1508−1512.
(8) Tian, N.; Zhou, Z. Y.; Sun, S. G.; Ding, Y.; Wang, Z. L. *Science* **2007**, *316*, 732−735.
(9) Solla-Gullon, J.; Vidal-Iglesias, F. J.; Lopez-Cudero, A.; Garnier, E.; Feliu, J. M.; Aldaza, A. *Phys. Chem. Chem. Phys.* **2008**, *10*, 3689−3698.
(10) Tao, A. R.; Habas, S.; Yang, P. D. *Small* **2008**, *4*, 310−325.
(11) Lee, I.; Delbecq, F.; Morales, R.; Albiter, M. A.; Zaera, F. *Nat. Mater.* **2009**, *8*, 132−138.
(12) Xia, Y. N.; Xiong, Y. J.; Lim, B.; Skrabalak, S. E. *Angew. Chem., Int. Ed.* **2009**, *48*, 60−103.
(13) Kang, Y. J.; Murray, C. B. *J. Am. Chem. Soc.* **2010**, *132*, 7568−7569.
(14) Kang, Y. J.; Ye, X. C.; Murray, C. B. *Angew. Chem., Int. Ed.* **2010**, *49*, 6156−6159.
(15) Zhang, J.; Yang, H.; Fang, J.; Zou, S. *Nano Lett.* **2010**, *10*, 638−644.
(16) Henzie, J.; Gruenwald, M.; Widmer-Cooper, A.; Geissler, P. L.; Yang, P. D. *Nat. Mater.* **2012**, *11*, 131−137.
(17) Li, Y.; Jiang, Y.; Chen, M.; Liao, H.; Huang, R.; Zhou, Z.; Tian, N.; Chen, S.; Sun, S. G. *Chem. Commun.* **2012**, *48*, 9531−9533.
(18) Wen, Y.; Fang, H.; Zhu, Z.; Sun, S. G. *Phys. Lett. A* **2009**, *373*, 272−276.
(19) Wang, C.; Daimon, H.; Lee, Y.; Kim, J.; Sun, S. H. *J. Am. Chem. Soc.* **2007**, *129*, 6974−6975.
(20) Lim, S. I.; Ojea-Jimenez, I.; Varon, M.; Casals, E.; Arbiol, J.; Puntes, V. *Nano Lett.* **2010**, *10*, 964−973.
(21) Zhang, J.; Fang, J. Y. *J. Am. Chem. Soc.* **2009**, *131*, 18543−18547.
(22) Zheng, H.; Smith, R. K.; Young-wook, J.; Kisielowski, C.; Dahmen, U.; Alivisatos, A. P. *Science* **2009**, *324*, 1309−12.
(23) Peng, Z. M.; Yang, H. *Nano Today* **2009**, *4*, 143−164.
(24) Maksimuk, S.; Teng, X.; Yang, H. *Phys. Chem. Chem. Phys.* **2006**, *8*, 4660−4663.
(25) Ahmadi, T. S.; Wang, Z. L.; Henglein, A.; El-Sayed, M. A. *Chem. Mater.* **1996**, *8*, 1161−1162.
(26) Burda, C.; Chen, X. B.; Narayanan, R.; El-Sayed, M. A. *Chem. Rev.* **2005**, *105*, 1025−1102.
(27) Wang, C.; van der Vilet, D.; Chang, K.-C.; You, H.; Strmcnik, D.; Schlueter, J. A.; Markovic, N. M.; Stamenkovic, V. R. *J. Phys. Chem. C* **2009**, *113*, 19365−19368.
(28) Wang, C.; Chi, M.; Li, D.; Strmcnik, D.; van der Vliett, D.; Wang, G.; Komanicky, V.; Chang, K.-C.; Paulikas, A. P.; Tripkovic, D.; Pearson, J.; More, K. L.; Markovic, N. M.; Stamenkovic, V. R. *J. Am. Chem. Soc.* **2011**, *133*, 14396−14403.
(29) Wang, C.; van der Vliet, D.; More, K. L.; Zaluzec, N. J.; Peng, S.; Sun, S. H.; Daimon, H.; Wang, G. F.; Greeley, J.; Pearson, J.; Paulikas, A. P.; Karapetrov, G.; Strmcnik, D.; Markovic, N. M.; Stamenkovic, V. R. *Nano Lett.* **2011**, *11*, 919−926.
(30) Schaak, R. E.; Sra, A. K.; Leonard, B. M.; Cable, R. E.; Bauer, J. C.; Han, Y. F.; Means, J.; Teizer, W.; Vasquez, Y.; Funck, E. S. *J. Am. Chem. Soc.* **2005**, *127*, 3506−3515.
(31) Buck, M. R.; Bondi, J. F.; Schaak, R. E. *Nat. Chem.* **2012**, *4*, 37−44.
(32) Fu, Q.; Weber, A.; Flytzani-Stephanopoulos, M. *Catal. Lett.* **2001**, *77*, 87−95.
(33) Si, R.; Flytzani-Stephanopoulos, M. *Angew. Chem., Int. Ed.* **2008**, *47*, 2884−2887.
(34) Rogach, A. L.; Talapin, D. V.; Shevchenko, E. V.; Kornowski, A.; Haase, M.; Weller, H. *Adv. Funct. Mater.* **2002**, *12*, 653−664.
(35) Sau, T. K.; Rogach, A. L. *Adv. Mater.* **2010**, *22*, 1781−1804.
(36) Sau, T. K.; Rogach, A. L.; Jaeckel, F.; Klar, T. A.; Feldmann, J. *Adv. Mater.* **2010**, *22*, 1805−1825.
(37) Wang, D. Y.; Kang, Y. J.; Doan-Nguyen, V.; Chen, J.; Kungas, R.; Wieder, N. L.; Bakhmutsky, K.; Gorte, R. J.; Murray, C. B. *Angew. Chem., Int. Ed.* **2011**, *50*, 4378−4381.
(38) Kang, Y. J.; Pyo, J. B.; Ye, X. C.; Gordon, T. R.; Murray, C. B. *ACS Nano* **2012**, *6*, 5642−5647.
(39) Kang, Y. J.; Qi, L.; Li, M.; Diaz, R. E.; Su, D.; Adzic, R. R.; Stach, E. A.; Li, J.; Murray, C. B. *ACS Nano* **2012**, *6*, 2818−2825.
(40) Chemseddine, A.; Weller, H. *Ber. Bunsen-Ges. Phys. Chem.* **1993**, *97*, 636−637.
(41) Murray, C. B.; Norris, D. J.; Bawendi, M. G. *J. Am. Chem. Soc.* **1993**, *115*, 8706−8715.
(42) Ohara, P. C.; Leff, D. V.; Heath, J. R.; Gelbart, W. M. *Phys. Rev. Lett.* **1995**, *75*, 3466−3469.
(43) Gelbart, W. M.; Sear, R. P.; Heath, J. R.; Chaney, S. *Faraday Discuss.* **1999**, *112*, 299−307.
(44) Park, K.; Koerner, H.; Vaia, R. A. *Nano Lett.* **2010**, *10*, 1433−1439.
(45) Song, Q.; Ding, Y.; Wang, Z. L.; Zhang, Z. J. *J. Phys. Chem. B* **2006**, *110*, 25547−25550.
(46) Demortiere, A.; Launois, P.; Goubet, N.; Albouy, P. A.; Petit, C. *J. Phys. Chem. B* **2008**, *112*, 14583−14592.
(47) Portales, H.; Goubet, N.; Sirotkin, S.; Duval, E.; Mermet, A.; Albouy, P.-A.; Pileni, M.-P. *Nano Lett.* **2012**, *12*, 5292−5298.
(48) Narayanan, R.; El-Sayed, M. A. *J. Am. Chem. Soc.* **2004**, *126*, 7194−7195.
(49) Narayanan, R.; El-Sayed, M. A. *J. Phys. Chem. B* **2005**, *109*, 12663−12676.
(50) Kang, Y. J.; Pyo, J. B.; Ye, X. C.; Diaz, R. E.; Gordon, T. R.; Stach, E. A.; Murray, C. B. *ACS Nano* **2013**, *7*, 645−653.
(51) Murray, C. B.; Kagan, C. R.; Bawendi, M. G. *Annu. Rev. Mater. Sci.* **2000**, *30*, 545−610.
(52) Murray, C. B.; Kagan, C. R.; Bawendi, M. G. *Science* **1995**, *270*, 1335−1338.
(53) Pileni, M. P. *Acc. Chem. Res.* **2012**, *45*, 1965−72.
(54) Bodnarchuk, M. I.; Kovalenko, M. V.; Heiss, W.; Talapin, D. V. *J. Am. Chem. Soc.* **2010**, *132*, 11967−11977.
(55) Rupich, S. M.; Shevchenko, E. V.; Bodnarchuk, M. I.; Lee, B.; Talapin, D. V. *J. Am. Chem. Soc.* **2010**, *132*, 289−296.
(56) Bibette, J. *J. Colloid Interface Sci.* **1991**, *147*, 474−478.
(57) Adzic, R. R.; Tripkovic, A. V.; Ogrady, W. E. *Nature* **1982**, *296*, 137−138.
(58) Clavilier, J.; Lamy, C.; Leger, J. M. *J. Electroanal. Chem.* **1981**, *125*, 249−254.
(59) Clavilier, J.; Parsons, R.; Durand, R.; Lamy, C.; Leger, J. M. *J. Electroanal. Chem.* **1981**, *124*, 321−326.
(60) Campbell, C. T.; Ertl, G.; Kuipers, H.; Segner, J. *J. Chem. Phys.* **1980**, *73*, 5862−5873.
(61) Berlowitz, P. J.; Peden, C. H. F.; Goodman, D. W. *J. Phys. Chem.* **1988**, *92*, 5213−5221.
(62) Gland, J. L.; Kollin, E. B. *J. Chem. Phys.* **1983**, *78*, 963−974.
(63) Su, X. C.; Cremer, P. S.; Shen, Y. R.; Somorjai, G. A. *J. Am. Chem. Soc.* **1997**, *119*, 3994−4000.
(64) Chen, M. S.; Cal, Y.; Yan, Z.; Gath, K. K.; Axnanda, S.; Goodman, D. W. *Surf. Sci.* **2007**, *601*, 5326−5331.
(65) Wang, Z. L.; Ahmad, T. S.; El-Sayed, M. A. *Surf. Sci.* **1997**, *380*, 302−310.